



# Simplifying biochemical signal transport in steady flows within a single-cell-trapping microchannel by linear low-order systems

Miao Yu<sup>1</sup> · Yong-Jiang Li<sup>2</sup> · Shu-Xin Liu<sup>1,3</sup> · Chun-Dong Xue<sup>2</sup> · Kai-Rong Qin<sup>1</sup>

Received: 11 April 2022 / Accepted: 30 December 2022 / Published online: 18 January 2023  
© The Author(s), under exclusive licence to Springer-Verlag GmbH Germany, part of Springer Nature 2023

## Abstract

Precise controlling and quantitative loading of dynamic biochemical stimulations to single cells are crucial for single cell dynamic analysis in vitro. Many microfluidic platforms have been proposed for providing spatiotemporal biochemical conditions. However, most existing investigations have ignored the effects of the transmission characteristics of biochemical signals within microchannels, leading to the difficulty in the quantitative and precise control of stimuli to targeted single cells. Herein, based on a single-cell-trapping microchannel with variable cross-sections, a simple and effective approach has been proposed to simplify the transmission system of biochemical signals within microchannel under steady flows by low-order linear systems. It is found that the third-order system is the most “cost-effective” choice, since the overall accuracy and robustness of the approximations, and the system simplicity are all satisfactory in this work. Moreover, the system parameters, gain and crossover frequency all vary linearly with the steady flow rate in the logarithmic coordinate, which has also been validated by fluorescein experiments. The simplifying approach could be universally applied to other mass-transfer systems theoretically for improving further research on the precise loading and controlling extracellular conditions in vitro in single cell analysis.

**Keywords** System identification · Linear low-order system · Transmission characteristics · Dynamic biochemical signal · Single cell dynamics · Microfluidics

✉ Yong-Jiang Li  
yongjiangli@dlut.edu.cn

✉ Kai-Rong Qin  
krqin@dlut.edu.cn

Miao Yu  
yumiao@mail.dlut.edu.cn

Shu-Xin Liu  
root8848@sina.com

Chun-Dong Xue  
xuechundong@dlut.edu.cn

<sup>1</sup> School of Biomedical Engineering, Faculty of Medicine, Dalian University of Technology, No. 2, Linggong Road, Dalian 116024, China

<sup>2</sup> School of Optoelectronic Engineering and Instrumentation Science, Dalian University of Technology, No. 2, Linggong Road, Dalian 116024, China

<sup>3</sup> Department of Nephrology, Affiliated Central Hospital of Dalian University of Technology, No. 826, Xinan Road, Dalian 116033, China

## 1 Introduction

Single cell analysis is a powerful and indispensable technological approach for gaining a deep understanding of cellular heterogeneity and discovering unique characteristics of individual cells (Altschuler and Wu 2010; Heath et al. 2016; Wen and Tang 2018). Quantitative analysis of single cell dynamics in response to biochemical signals is developed to be a novel point of penetration of single cell analysis recently (Spiller et al. 2010). It would provide more comprehensive dynamic and quantitative information for the mechanism exploration of serious diseases, disease diagnosis and drug evaluation, etc.

Microfluidic technology has emerged as an important tool for precisely quantitative analysis of single cell dynamics in response to biochemical signals owing to the advantages in single cell manipulation, analogy of extracellular environment, comparable scale to cell diameters, as well as cellular behavior monitoring (Roper 2016; Guo et al. 2020; Kim et al. 2021). Trapping single cells and precise loading

dynamic biochemical signal to them are prerequisite for microfluidic single cell dynamic analysis. Many microfluidic platforms capable of capturing or manipulating single cells (Bai et al. 2013; Lee et al. 2018; Lipp et al. 2021; Tan et al. 2020; Guo et al. 2016; Silverio et al. 2017; Gao et al. 2019) and providing dynamic biochemical stimulating conditions (Tay et al. 2010; Chingozha et al. 2014; Garcia et al. 2015; Song et al. 2018; Chen et al. 2017, 2018; Kim et al. 2021; Gao et al. 2019) have been proposed. However, most of the existing approaches only pay attention to how to generate the diverse dynamic biochemical stimulating signals. While, the signal single cells received are not exactly the same as the biochemical signals generated at the entrance, since specific distance exists between the single cell traps and the entrance. Some investigations have focused on the transport mechanism of the dynamic signals within microchannels recently, revealing that the microchannels act as low-pass filters, the dynamic signals transporting within them are attenuated and time-delayed (Beard 2001a, b; Lam et al. 2005; Xie et al. 2008; Azizi and Mastrangelo 2008; Azizi et al. 2010; Li et al. 2013; Chen et al. 2017; Li et al. 2018). Therefore, quantitative analysis of the transmission characteristics of biochemical signals within microchannels is indispensable for quantitatively loading dynamic biochemical stimulating signals to single cells and further precisely mimicking or even controlling the physiological microenvironment *in vitro* for single cell dynamic analysis.

To date, bulk of transmission analysis theories were only appropriate for the uniform microchannels with rectangular cross-sections (Beard 2001a, b; Lam et al. 2005; Xie et al. 2008; Azizi and Mastrangelo 2008; Azizi et al. 2010; Li et al. 2013; Chen et al. 2017; Li et al. 2018), incapable of the microchannels with varying cross-sections or other complicated microstructures. To this end, our group took a step forward and analyzed the transport mechanism of dynamic signals in steady and non-reversing pulsatile flows in a single-cell-trapping microchannel with varying cross-section (Yu et al. 2019). Due to the streamline-shaped microchannel design (Yu et al. 2016), the simplified 2D time-dependent Taylor–Aris dispersion governing the longitudinal and transverse molecular diffusion within the microchannel could be derived (Yu et al. 2019). It is a partial differential equation without analytic solution, other than the governing equations for the rectangular or Y-shaped channels which can be analytically solved (Li et al. 2013, 2018). That is, the transmission characteristics within the microchannel can only be analyzed by numerical solution, which is complicated, well mathematical-knowledge-required, and long time-consuming (hours or days) due to the numerical differentiation and multidimensional matrix calculation. For other single-cell-analysis microchannels or microwells with specific microstructures, the 3D convection–diffusion equation is difficult to be simplified, let alone analytical solved; thus, to explore

the transport mechanism, only more time-consuming 3D numerical simulation methods [such as the computational fluid dynamic (CFD) package FLUENT or COMSOL] can only be approached. Moreover, without the analytical solution, i.e., the transfer function of micro-transport system, it is difficult or even impossible to integrate external feedback controller for precise control (Na et al. 2020; Recktenwald et al. 2021). Thus, it is essential and urgent to develop a novel approach to analyze the transport mechanism of dynamic signals within the microchannel simply and rapidly, and applicable for further precisely controlling the extracellular stimulating signals in the single cell analysis.

In the field of signal system, several well-developed system identification methods can be used to obtain the approximate transfer function of a black box system, once the input and output signals are prior known. Generally, linear low-order systems, especially second-order or third-order system, are selected to capture the transmission characteristics, since their system features and physical meanings are clear. They are also suitable for biomicrofluidics applications (Kniss-James et al. 2017). In this work, take the single-cell-trapping microchannel our group proposed as an example (Fig. 1a), linear low-order system expressed by few numbers of parameters was introduced to approaching this complicated micro-transport system. Due to the flow-dependent feature of the transport system, investigations under steady flows were first focused herein. Input–output data sets gained from the 2D numerical simulation with varying input frequencies, amplitudes, and waveform types in steady flows were adopted for the system identification. Additionally, Gaussian white noises with varied Signal-to-Noise Ratios (SNR) were included to the simulation data sets to better simulate the physical existing and ineradicable uncertainties in the relevant individual variables in this work. To increase the universality of this simplification, the relationships between the system parameters and flow rate were investigated and validated by fluorescein experiments. This simple and convenient method can be expected to improve further research on the precise loading and controlling extracellular conditions *in vitro* in single cell analysis.

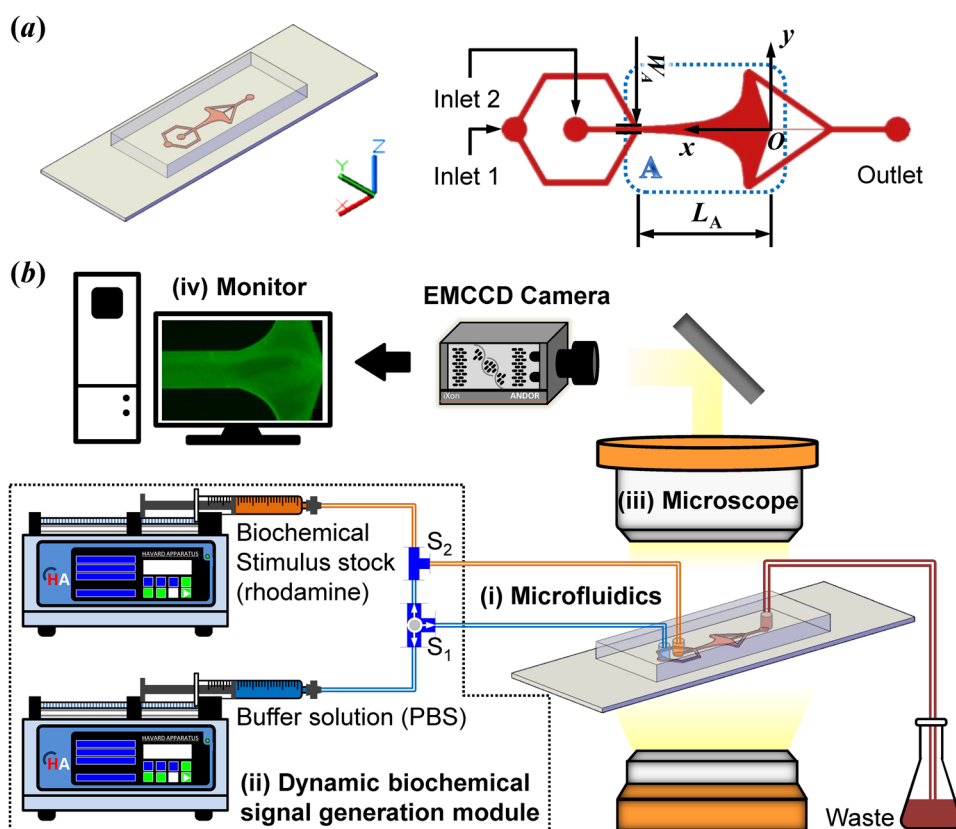
## 2 Materials and methods

### 2.1 Hydrodynamic model for the transport system within the single-cell-trapping microchannel

#### 2.1.1 Governing equation

To trap single cell and further explore single cell dynamics in response to precise biochemical stimulations, we proposed a microfluidic single-cell-trapping device using a combination of stagnation point flow and boundary effect,

**Fig. 1** Schematic representations of the microfluidic devices. **a** Design of the previous PDMS-glass microfluidic single-cell-trapping device, comprises a single-cell-trapping microchannel A, two inlets and one outlet (Yu et al. 2016). The coordinate system used in the subsequent analysis is consistent with that shown here, where *O* is the origin. **b** Schematic diagram of experimental setup, mainly contains four parts: (i) microfluidic chip, (ii) dynamic biochemical signal generation module controlled by the programmable syringe pumps, (iii) real-time observation module (microscope), and (iv) display, record and data analysis module, and monitor



as shown in Fig. 1a (Yu et al. 2016). The single-cell-trapping microchannel A is the “only way” for loading the precise biochemical signals to the trapped single cell; that is, it is a micro-transport system. The soluble biochemical molecules within this microchannel A are transported and mixed by convection and diffusion. Due to the streamline-shaped design of the microchannel A (Yu et al. 2016), by combining the convection–diffusion equation and the flow governing Navier–Stokes equation, the governing equation of the height-averaging concentration of biochemical stimulus,  $\bar{\phi}$ , i.e., the 2D time-dependent Taylor–Aris dispersion with longitudinal and transverse molecular diffusion in the microchannel A can be known and expressed in the polar coordinate system as (Yu et al. 2019)

$$\frac{\partial \bar{\phi}}{\partial t} + U_r \frac{\partial \bar{\phi}}{\partial r} + \frac{U_\theta}{r} \frac{\partial \bar{\phi}}{\partial \theta} = D_1 \frac{1}{r} \frac{\partial \bar{\phi}}{\partial r} + D_2 \frac{\partial^2 \bar{\phi}}{\partial r^2} + D_3 \frac{1}{r^2} \frac{\partial \bar{\phi}}{\partial \theta} + D_4 \frac{1}{r^2} \frac{\partial^2 \bar{\phi}}{\partial \theta^2}, \tag{1}$$

where

$$\begin{aligned} D_1 &= D + \frac{n-1}{210} \frac{H^2 U_r^2}{D} + \frac{n}{210} \frac{H^2 U_\theta^2}{D} \\ D_2 &= D + \frac{1}{210} \frac{H^2 U_r^2}{D} \\ D_3 &= \frac{n-1}{105} \frac{H^2 U_r U_\theta}{D} \\ D_4 &= D + \frac{1}{210} \frac{H^2 U_\theta^2}{D}, \end{aligned} \tag{2}$$

where *n* is a positive number greater than 1, *D* is the diffusion coefficient, and *U<sub>r</sub>* and *U<sub>θ</sub>* are the radial and circumferential components of the height-averaging velocity  $\vec{U}$ , and they are functions of the width *W<sub>A</sub>* and length *L<sub>A</sub>* of microchannel A (Yu et al. 2019)

$$\begin{aligned} U_r &= \frac{Qnr^{n-1} \cos(n\theta)}{2Hr_0 \sin(n\theta_0)} \\ U_\theta &= -\frac{Qnr^{n-1} \sin(n\theta)}{2Hr_0 \sin(n\theta_0)}, \end{aligned} \tag{3}$$

where  $r_0 = \sqrt{L_A^2 + \frac{W_A^2}{4}}$ , and  $\theta_0 \approx \arctan \frac{W_A}{2L_A}$ ; *Q* is the flow rate

Since Eq. 1 is a partial differential equation without analytic solution, the transmission characteristics of the

biochemical signal within the microchannel A can be obtained only by numerical methods (Yu et al. 2019). Furthermore, the transportation process depends on the geometrics of microchannel A ( $L_A$ ,  $W_A$  and  $H_A$ ) and the input flow rate  $Q$  (Eqs. 1-3). That is, microchannels with different geometric sizes under different flow rates should correspond to different transport systems. In this work, the size of microchannel A was determined and invariant based on the considerations of the space efficiency of the entire microfluidics design and the further high-throughput study (Table 1). While, the value of the flow rate  $Q$  varied according to the experimental conditions, aiming to discover the variation features of the system characteristics with the flow rate.

2.1.2 Numerical simulation

To attain the input–output data for system identification, the Taylor–Aris dispersion (Eq. 1) was numerically solved in MATLAB (The Math Works R2020a, Inc). In this work, the Peaceman–Rachford (P–R) scheme was used in the approximation of the solution of Eq. 1 (Yu et al. 2019).

In default, the inlet flow was set to be a steady flow. Additionally, the concentrations of the biochemical stimulations at the inlet (i.e., the input signal) were divided into two categories: pure signals and noise signals. Typically, the pure signals were set as

$$\phi(t) = \phi_0 [1 + \delta F_{\text{wave}}(2\pi f_c t)], \tag{4}$$

where  $\phi_0$  is the average concentration,  $F_{\text{wave}}$  represents the waveform function, and several waveform types are selected including the single-frequency signal (sine) and multiple-frequency signals (square, triangle, pulse-like, step). And  $\delta$  is the amplitude, and  $f_c$  is the frequency of the biochemical signal. And, they are also variable, ranging from 0.01 Hz to 2 Hz, and 0.2 to 1, respectively. The frequency  $f_c$ , amplitude  $\delta$  and the waveform type of the biochemical signals are controlled to be single varied. To improve the accuracy of subsequent linear system identification, one multiple-frequency signal, the square waveform, is picked to be the

default waveform. Other default values are listed in Table 1. Unless otherwise specified, these default values are adopted throughout the simulation work.

Furthermore, to improve sample diversity and to better simulate the physical irreducible uncertainties in the relevant individual variables in this work, Gaussian white noises with varied SNRs are added to the input biochemical stimulations to generate the noise signals. Herein, the noise signals were set as

$$\phi(t) = \phi_0 [1 + \delta \sin(2\pi f_c t)] + G_{\text{noise}}(\text{SRN}, t), \tag{5}$$

where the frequency  $f_c$  and the amplitude  $\delta$  of the original signal are both default values listed in Table 1.  $G_{\text{noise}}(\text{SRN}, t)$  is the Gaussian white noise with SNR ranging from 30 to 10.

In all the simulations described below, the default output observation position is the location around the trapped single cell, which is assumed to be  $15\mu\text{m}$  from the trap point (origin of coordinate in Fig. 1), i.e.,  $x = 15\mu\text{m}$  and  $y = 0$  ( $r = 15\mu\text{m}$  and  $\theta = 0$ ). That is, the output signal is the concentration of the biochemical stimulation detected at  $15\mu\text{m}$  from the trap point.

Overall, the simulation lasted from a few minutes to dozens of hours according to the simulation conditions.

2.2 Simplified model for the transport system by linear low-order systems

As mentioned in Sect. 2.1, this transport system within the single-cell-trapping microchannel A is complicated and nonlinear; and the numerical calculations are generally time-consuming. For most real nonlinear biological, mechanical, or other complex systems, they universally could be simplified by linear order systems (Venkat et al. 2003; Bai 2008; Kniss-James et al. 2017) and their transfer functions satisfy

$$H(s) = \frac{K \prod_{i=0}^{n_z} (s - z_i)}{\prod_{i=0}^{n_p} (s - p_i)}, \tag{6}$$

where  $K$  is the system gain,  $n_z$  is the number of zeros ( $z_i$ ) for the system, and  $n_p$  is the number of poles ( $p_i$ ), i.e., the order of the system. It also can be expressed as

$$H(s) = \frac{\sum_{i=0}^{n_z} (a_i s^i)}{s^{n_p} + \sum_{j=0}^{(n_p-1)} (b_j s^j)}, \tag{7}$$

where  $a_i$  is the numerator coefficient, and  $b_j$  is the denominator coefficient of the system. Absolutely,  $K = a_{n_z}$ .

To simplify the numerical calculation and better understand the transmission characteristics of the biochemical signals within this transport system (microchannel A) for further precisely controlling the system, a linear system which is expressed by Eq. 7 was adopted to approximate.

Table 1 Default values of the flow and biochemical stimulation parameters used in the numerical simulations

Parameters	Values
$n$	2.5
$L_A$	200 $\mu\text{m}$
$W_A$	80 $\mu\text{m}$
$H_A$	25 $\mu\text{m}$
$D$	$4.14 \times 10^{-10} \text{ m}^2/\text{s}$
$Q$	$1 \times 10^{-12} \text{ m}^3/\text{s}$
$\phi_0$	$1 \times 10^{-3} \text{ mol}/\text{m}^3$
$f_c$	0.5 Hz
$\delta$	0.5

Once the input flow rate changes, the system renews, i.e., the features of the approximating linear system, including values ( $a_i$  and  $b_j$ ) and numbers ( $n_z$  and  $n_p$ ), vary with the flow rate. Due to the indeterminacy on the selection of system order, second-order, third-order, and fourth-order systems were all adopted under each flow rate, respectively, at the beginning.

More detailedly, for each flow rate condition (totally 9 flow rates,  $Q = 1, 2, 5, 8, 10, 20, 50, 80, \text{ or } 100 \times 10^{-13} \text{ m}^3/\text{s}$ ), 6 kinds of pre-selected linear systems were employed, including second-order system with 1 zero ( $n_z = 1, n_p = 2$ ), third-order systems with 1 or 2 zeros ( $n_z = 1, n_p = 3$  or  $n_z = 2, n_p = 3$ ), and fourth-order systems with 1 to 3 zeros ( $n_z = 1 \text{ to } 3, \text{ and } n_p = 4$ ). That is, the total number of the system parameters,  $N_{\text{para}}$ , which satisfies  $N_{\text{para}} = n_z + n_p + 1$ , ranges from 4 to 8. For each pre-selected linear system, 18 “pure” input–output simulation data sets with varying input frequencies (8 groups,  $f_c = 0.01, 0.02, 0.05, 0.1, 0.2, 0.5, 1, \text{ and } 2 \text{ Hz}$ ), amplitudes (5 groups,  $\delta = 0.2, 0.4, 0.6, 0.8, \text{ and } 1$ ) and waveform types (5 groups, single-frequency: sine, multiple-frequency: triangle, square with opposite phase from the default one, pulse-like, and step), and 5 “noise” input–output data sets with varying SNRs (SNR = 30, 25, 20, 15 and 10) were applied to determine the optimal parameters of the each approximating linear system with minimum averages of mean relative error (MRE,  $\frac{|\text{Output}_{\text{simulation}} - \text{Output}_{\text{identification}}|}{\text{Output}_{\text{simulation}}} \times 100\%$ ) and mean squared error (MSE). The entire system identification process was accomplished by combining the System Identification Toolbox 9.12 and self-coded MATLAB scripts, see the flowchart shown in ESI Fig. S1 for details. Statistical analysis was performed using OriginPro software (OriginLab Corporation, Northampton, MA, USA).

## 2.3 Experimental validation

### 2.3.1 Microfluidics fabrication and apparatus

To validate the identification effect experimentally, a microfluidic chip was made. All the microchannels were patterned in PDMS (Sylgard 184, DOW CORNING) by replica molding. The mold was entrusted to a specialized microchip manufacturing company (ZhongXinQiHeng, Suzhou, China) for production. Next, the microchannel layer was obtained by pouring PDMS with 10 : 1 (v/v) base : crosslinker ratio onto the mold yielding a thickness of 3.5–4 mm approximately. After curing the elastomer for 2 h at 70 °C, the PDMS slab was peeled from the mold, punched, and hermetically bonded to a coverslip by plasma oxidation.

The two inlets of the fabricated microfluidic chip were coupled connected with two programmable syringe pumps (Pump 11 Elite, Harvard Apparatus, MA, USA) filled with the biochemical stimulus stock and buffer solution by two

T-bends,  $S_1$  and  $S_2$  (Fig. 1(b)).  $S_1$  is switchable and  $S_2$  is always on. By controlling the on–off state of  $S_1$ , the buffer solution can be flow into the microchannels directly through inlet 1 to flush the microchannels at the beginning or wash out the residual fluorescein, or mixed with the biochemical stimulus stock to generate the dynamic biochemical stimulation flowing into the microchannel through inlet 2. And arbitrary biochemical signals can be generated by controlling the flow rates of the two solutions (see ‡ESI Text T1 for details) (Yu et al. 2016). The flow and concentration fields within the microchannel were observed under an inverted fluorescence microscope (IX73, Olympus, Tokyo, Japan) with a high-speed EMCCD camera (iXon Life EMCCD, Andor, UK) in real time.

### 2.3.2 Fluorescein experimental protocol

For the experimental verification, one type of fluorescein, rhodamine 6G (Sigma-Aldrich, St. Louis, MO, USA) was used to mimic biochemical stimulations. It was dissolved in phosphate-buffered saline (PBS) to form a stock solution with a concentration of 5  $\mu\text{mol}/\text{mL}$ , which was in the linear range between fluorescence intensity and its concentration (see ‡ESI Fig. S2). The switch  $S_1$  was turned to the inlet 2. The flow rates of two programmable syringe pumps were set to wave as two expected and time-dependent functions, and finally generated a biochemical stimulation solution with expected average concentration, frequency and flow rate; see the detailed implementation in ‡ESI T1. And then, the fluorescence intensities at different regions of interest (ROIs, the entrance of microchannel A and near the cell trap) were measured and analyzed by describing the variation of the average gray value of ROIs with time in MATLAB.

## 3 Results

### 3.1 Comparison of system identification effects under different pre-selected linear systems

Due to the lack of referable prior experiences on transport system identification, it is indeterminate that which kind of linear system is the best one for approximating the transmission characteristics of this single-cell-trapping microsystem. Thus, in this work, second-order, third-order, and fourth-order systems with parameters ranging from 4 to 8 were pre-selected. First, the system identification effects under different pre-selected linear systems were compared. As mentioned in Sect. 2.2, 18 “pure” and 5 “noise” input–output data sets under 9 flow rates were initially used for the system identification. First, to clarify the effect of the noise signal on the stability of system identification, 162 groups (18  $\times$  9) of “pure” input–output data sets and 207 groups

(23 × 9) of “mix” (pure+noise) input–output data sets were used for identifying each pre-selected system parameters, respectively. Thus, each pre-selected system has two kinds of identified system parameters: without-consideration and with-consideration of noise. Based on these two kinds of identified system, all the 207 groups of simulation data sets were introduced to testify the approximation effects of these two systems, respectively. Finally, two groups of MRE data (207/group) and MSE data (207/group) were obtained under each selection of the identified system. We found that the distributions and variation trend of MREs and MSEs are basically consistent; thus, only MRE data are shown herein. With consideration of the uncertainties in the relevant individual variables, i.e., involving noises into the data sets in the modeling, the identified system is closer to the real transport system. MRE decreases generally (see ‡ESI Fig. S3), indicating that the influences of the uncertainties of mainly relevant individual variables in this work and their propagation into the system identification can be effectively reduced by introducing noise to the data sets. Therefore, all the results shown below are obtained based on the model with consideration of noise.

To totally compare the approximation effect of each pre-selected system, the distributions of MREs under 9 flow rates for each system are shown in Fig. 2. In the second-order system approximation, the MRE distribution range is the largest; values are the most scattered. That is, the approximating effect is unstable using second-order system. With the increase of the parameter number or order of the

system, the approximating effects, both the MRE value and the overall distribution, improve significantly. Moreover, it is obvious that increasing the pole number (i.e., system order) is better than increasing the zero number on the improvement of approximation, comparing the MRE distributions of the two cases under 6 system parameters [the third-order system with 2 zeros,  $n_z = 2, n_p = 3$  and the fourth-order system with 1 zero,  $n_z = 1, n_p = 4$ ] with the case under 5 system parameters ( $n_z = 1, n_p = 3$ ), respectively. From the point of the average value of MERs, with the increase of one zero, the mean of MREs decreases but no more than 2.5% for the same order system; and the higher order, the less decrease. While, keep zero number (for instance,  $n_z = 1$ ) the same and increase the order (pole number,  $n_p = 2$  to 4), the error becomes lower more dramatically, especially between the second-order and third-order systems, the averaging-MRE difference is even higher than 2.3%. Specifically, MREs are universally less than 2% and bulk of them are even lower than 5% for the fourth-order system approximation. And almost 75% of them are less than 1% when approximating by the third-order system. However, higher order leads to the increase of the system complexity. Overall, the third-order system with 1 zero ( $n_z = 1, n_p = 3$ ) performs well. Thus, it could be the most “cost-effective” choice to approximate the transport system within this single-cell-trapping micro-channel, with comprehensive considerations of the goals for both less MRE and lower system order (fewer system parameters). Unless otherwise specified, the results shown below are the approximations by the third-order system with 1 zero.

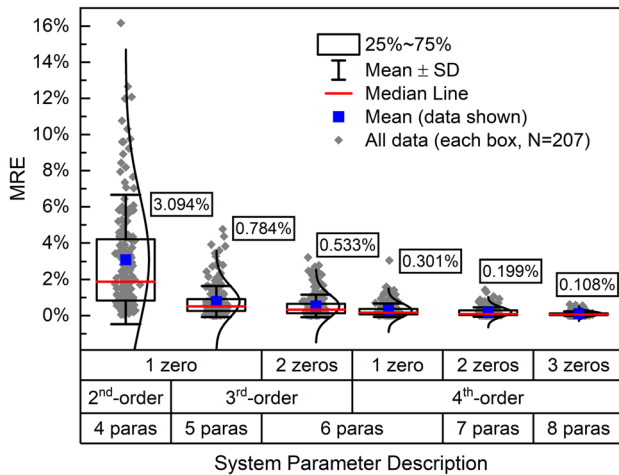


**Fig. 2** Box plots of the MRE distributions for the system identification by different pre-selected linear systems. The total number of the system parameters (abbr, paras),  $N_{para}$  range from 4 to 8. Data shown in each box includes all the flowing (9 flow rates) and biochemical stimulating (23 input–output data sets) conditions; thus,  $N = 207$ . The mean of MREs for each pre-selected system is labeled (blue square dot) and shown above each box; and red lines represent the medians

### 3.2 Representative approximations by third-order system

As mentioned in Sect. 2.2, the 23 groups of input–output simulating data (pure signals with varying  $f_c, \delta$  and waveform, and noise signals with varying SNRs) were adopted to determine the optimal parameters of the third-order system ( $a_1, a_0, b_2, b_1$  and  $b_0$ ). To observe the approximating effects more directly, the identified results corresponding to the 23 inputs under the default flow rate by the optimal third-order system are shown; see Figs. 3, 4, 5, and 6.

As shown in Fig. 3, the approximations by third-order system generally perform well from the point of time-domain. The overall MREs are almost within the acceptable range (< 5%), see Fig. 2 and ‡ESI Fig. S4; and the frequencies, amplitudes and phases of the identified outputs mainly match those of the simulation results, other than few cases. In details, when low-frequency signal inputs ( $f_c = 0.01\text{Hz}$ ), the output frequency and phase between the approximation and simulation are both not significantly different. And their amplitudes are also almost equal, only weak and ignorable overshoot and undershoot near the rising edge and the falling edge, see the subgraph (E-1) in Fig. 3. It is a universal

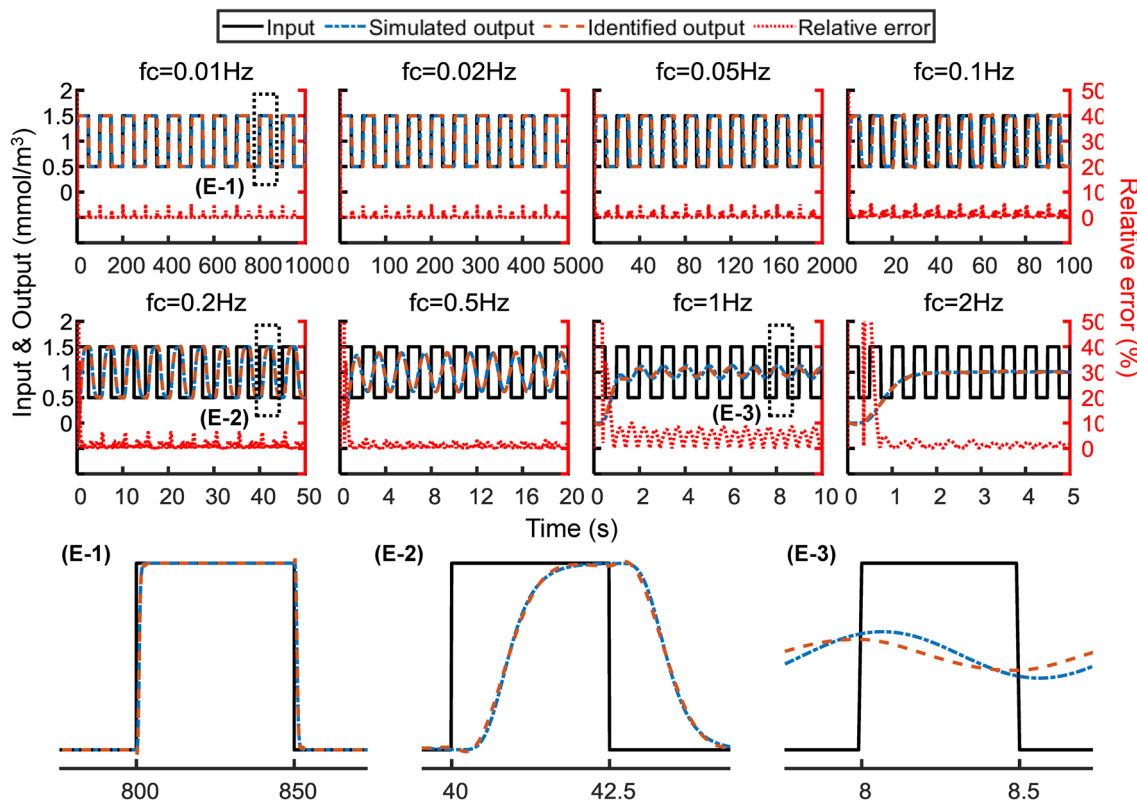


**Fig. 3** Comparisons of the biochemical output signals between numerical simulation and identification by third-order system, under different input signals with varying frequencies,  $f_c$ . The flow rate, input amplitude ( $\delta$ ), and waveform are the default ones listed

in Table 1. Left axis: input and outputs; right axis: the relative error between simulation and identification. (E-1) to (E-3) are the partial enlarged versions of the results corresponding to  $f_c = 0.01\text{Hz}$ ,  $f_c = 0.2\text{Hz}$ , and  $f_c = 1\text{Hz}$  in about one period, respectively

phenomenon for the linear system and would recede with the increase of input frequency. Consequently, the identified output amplitude and phase become distinguishable slightly from that of the simulations, see the individual case shown in the subfigures (E-2) and (E-3). While, the output frequencies still can be matched with each other.

Similarly, the approximating effects are slightly different with the variation in the input amplitude,  $\delta$  (Fig. 4). The frequencies of the identified and simulating results match, regardless of the input amplitude. And varying  $\delta$  has a negligible effect on the identified output amplitude, compared to the varying-frequency cases. Only the difference of the output phases can be recognized by “magnifying glass”; see the two subgraphs (E-1) and (E-2) in Fig. 4. Thus, the gradually increasing error is primarily caused by the decreasing trough value with the increase of  $\delta$ .

Further, we compared the approximating performances under various input waveforms, including single-frequency signal and multiple-frequency ones. Figure 5 shows that the approximation under single-frequency input (sinusoidal) is better than multiple-frequency ones. And identification performance is almost impervious to the input phase, comparing the results shown in Fig. 3 ( $f_c = 0.5\text{Hz}$ ) and Fig. 5

(square+ $\pi$ ), which input phases are opposite. For the input with a shorter pulse period, the approximation by the third-order system is still impressive. The output frequency, phase, and amplitude of the identification and simulation are nearly undifferentiated, and only the mean value is lower; see (E-1) in Fig. 5. More meaningfully, the step responses of the transport system and the identified third-order system are comparable. Inapparent overshoot and undershoot exist near the rising edge and the falling edge. Thus, these two systems should have the greatly similar characteristics both in time-domain and frequency-domain theoretically.

In addition to the “pure” data, the identification model was constructed with consideration of Gaussian white noise. Similar to the approximation performances under “pure” input signal, the identified output almost overlaps the simulating result, regardless of the level of SNR, as shown in Fig. 6. MREs are all lower than 1%, and increase slightly (lower than 2%) with the increase of SNR. The difference between the identified result and the simulating output is difficult to recognize only by eyes, although SNR is quite small; see the subgraph (E-1) in Fig. 6. Thus, it can be concluded that the identified model should also be effective for

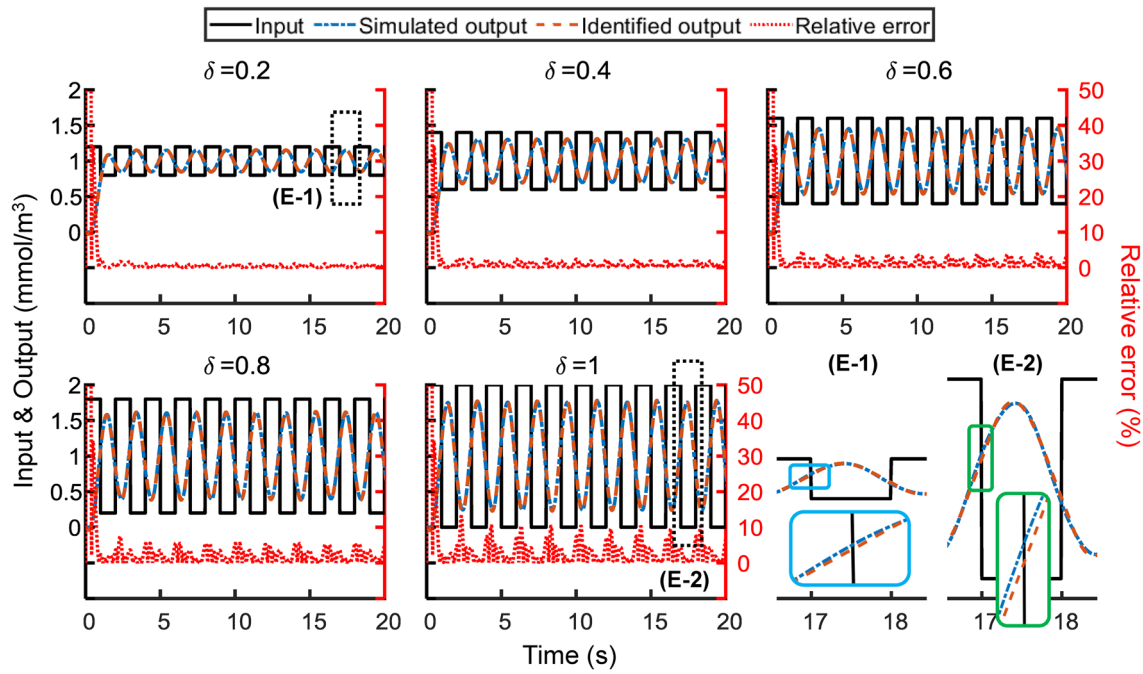


**Fig. 4** Comparisons of the biochemical output signals between numerical simulation and identification by third-order system, under different input signals with varying amplitudes,  $\delta$ . The flow rate, input

frequency ( $f_c$ ), and waveform are the default ones listed in Table 1. (E-1) and (E-2) are the partial enlarged versions of the representative results corresponding to  $\delta = 0.2$  and  $\delta = 1$ , respectively

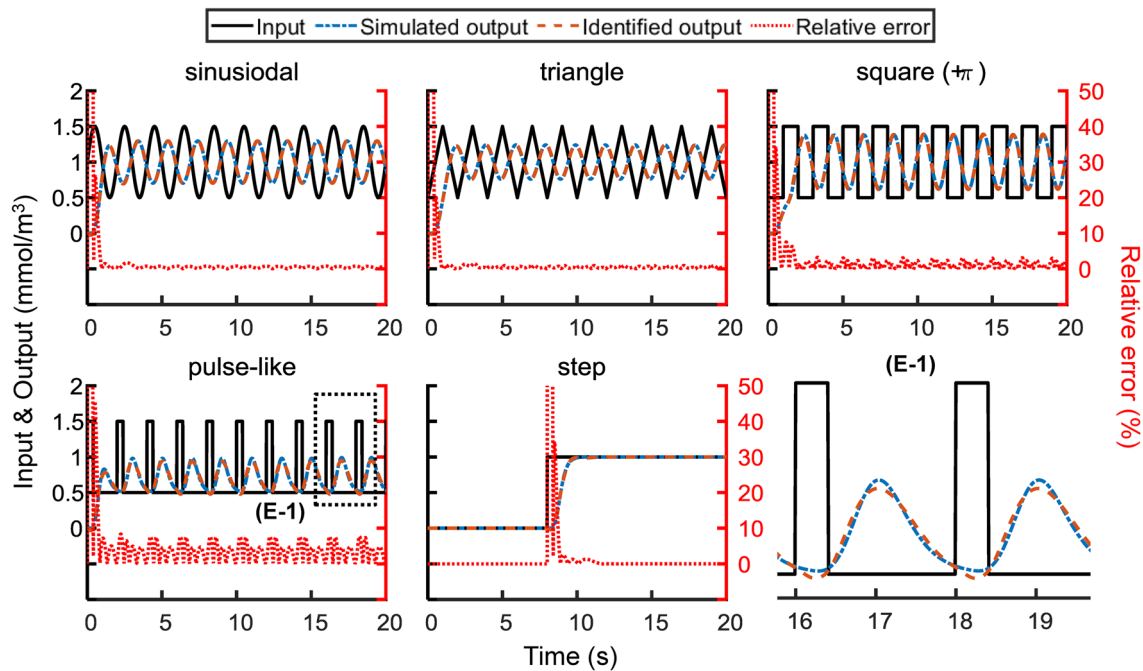


**Fig. 5** Comparisons of the biochemical output signals between numerical simulation and identification by third-order system, under different input signals with varying waveforms, including sinusoidal,

triangular, square with opposite phase, pulse-like, and step waves. Here,  $f_c = 0.5\text{Hz}$ ,  $\delta = 0.5$ . (E-1) is the partially enlarged version of the pulse-like result



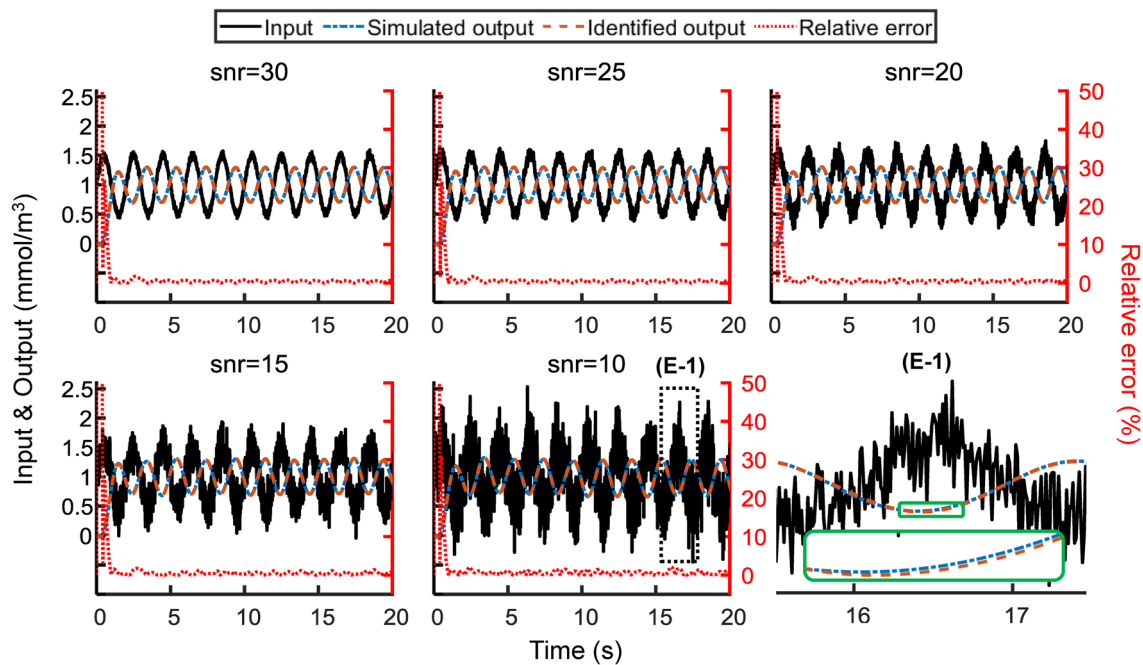


**Fig. 6** Comparisons of the biochemical output signals between numerical simulation and identification by third-order system when inputting different noise signals with varying SNR. Here,  $f_c = 0.5\text{Hz}$ ,

$\delta = 0.5$ . (E-1) is the partially enlarged version when inputting signals with large amount of noise

the experimental data which contains systematic and random uncertainties.

The approximation effects in time-domain have been shown and expounded detailedly (3, 4, 5 and 6). And the amplitude–frequency characteristics of the micro-transport system are also preliminarily investigated by analyzing the characteristic frequency of the identified third-order system. Data are shown in the subsequent section.

In Figs. 3, 4, 5 and 6, the inputs adopted to determine the optimal parameters of the third-order system are all simple ones with regular frequency. To further numerically validate the accuracy and the robustness of this optimal third-order system, more complex input–output data should be introduced. And the potential application of this study is to quantitatively load dynamic biochemical/physicochemical stimulations for single cell analysis. While, the cellular microenvironment in vivo is quite complex and diverse. Some of the dynamic stimuli applied to biological cells are the signals with time-varying frequency and/or amplitude, such as the blood glucose (Brownlee and Hirsch 2006). Some are more rhythmic, such as the arterial pulse wave. Therefore, a signal with time-varying frequency and amplitude and a physiological-shaped signal were chose herein. In Fig. 7a, the identification result is eminently precise from the beginning to about 80 s; and the difference in the output amplitude and phase occurs, especially in the amplitude, once the input frequency becomes higher (nearly 1Hz).

While, these errors could be acceptable for the application that the amplitude is the not extremely interested feature. Moreover, for the physiological-shaped signal, the third-order system identification result almost captures all the amplitude, frequency, and phase characteristics, although the input frequency is not much low. Merely, the waving of the peak is slightly different; see the details in Fig. 7b. In summary, the third-order system (with 1 zero) could be adopted to approximate the transmission characteristics of the transport system precisely in most instances.

### 3.3 Log–log linear relationships between system parameters, characteristic values, and flow rate

Data shown in Sect. 3.2 have adequately demonstrated that under the default flow rate, the transmission characteristics of the biochemical signal transporting in the mass-transfer system (microchannel A) could be captured by a third-order system (Figs. 3, 4, 5, 6 and 7). Similarly, under other flow rates, higher or lower, the approximations by third-order system still perform gratifyingly, either the MRE distribution or the output features (such as frequency, amplitude, and phase); see Fig. 2, and ‡ESI Figs. S4, S5. The universal, flow-independent applicability of the third-order system approximating this transport system raises a question that, might the system parameters and characteristic values, such as the crossover frequency ( $f_{sc}$ ,

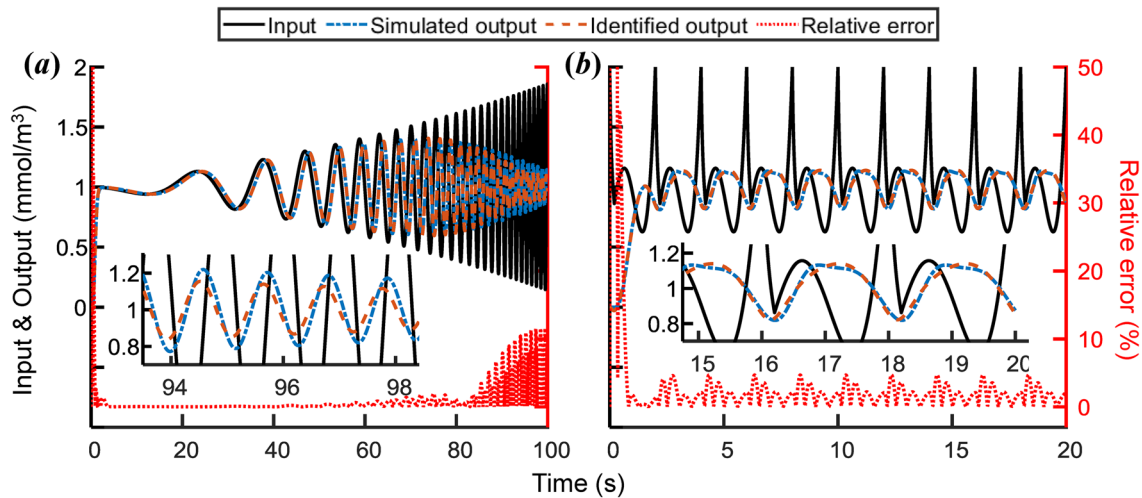


**Fig. 7** Validation of the identified third-order system with optimal parameters. **a** An input with time-varying frequency and amplitude. **b** A physiological-shaped input. The flow rate is the default one, that  $Q = 1 \times 10^{-12} \text{m}^3/\text{s}$ . Details are shown in the enlarged subgraphs

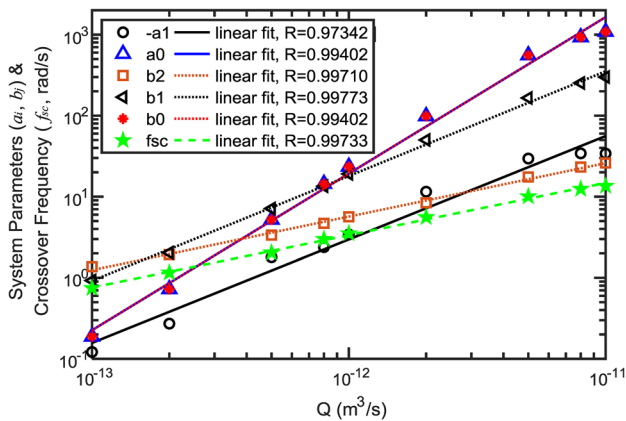


**Fig. 8** Variations of the parameters ( $a_i$  and  $b_j$ ) and the crossover frequencies ( $f_{sc}$ ) of the identified third-order system with the flow rate  $Q$  in the logarithmic coordinate. The lines with different linetypes and colors are the linear approximations to the corresponding data, and R-squared, on behalf of the fitting effects, are listed, respectively

the frequency where the gain margin is measured, which is a  $-180^\circ$  phase crossing frequency, unit: rad/s) and the gain ( $K$ ), monotonically or even functionally vary with the flow rate? To address this question, we performed curve fitting analysis on the parameters,  $a_i$  and  $b_j$ , and the crossover frequency,  $f_{sc}$  of the optimal third-order system under each flow rate  $Q$ . Ultimately, we found that,  $a_i$ ,  $b_j$ ,  $f_{sc}$  and  $K$  ( $K = a_n$ ) all approximately increase linearly with the increase of  $Q$  in the logarithmic coordinate, as shown in Fig. 8. Here, for the third-order system with 1 zero, all the denominator coefficients  $b_j$  are positive, while the numerator ones  $a_i$  are not ( $a_1 < 0$ ). Thus, the log–log linear fitting

functions between the parameters and the flow rate can be expressed as

$$\lg |a_i| = p_{i1} \lg(Q) + p_{i2} \tag{8}$$

and

$$\lg(b_j) = q_{j1} \lg(Q) + q_{j2}, \tag{9}$$

where  $a_i$  ( $i = 1$  or  $0$ ) and  $b_j$  ( $j = 2, 1$  or  $0$ ) are the numerator coefficient and the denominator coefficient of the system, respectively (Eq. 7);  $p_{i1}$ ,  $p_{i2}$  and  $q_{j1}$ ,  $q_{j2}$  are the log–log linear fitting coefficients for  $a_i$  and  $b_j$ , respectively. Similarly, the function between the crossover frequency,  $f_{sc}$ , and the flow rate,  $Q$ , performs in the same way as Eq. 8 or 9, with different fitting coefficients, as well as the system gain,  $K$ , which is actually equal to  $a_1$ .

In terms of linear fitting performance, the fitting lines corresponding to the coefficients ( $a_i$  and  $b_j$ ) of the same orders, are approximately parallel, i.e.,  $p_{i1} \approx q_{j1}$  ( $i = j = 1$  or  $0$ ), labeled as  $L_{a_i} \parallel L_{b_j}$ ; specially, for the constant terms ( $a_0$  and  $b_0$ ), they almost coincide, i.e.,  $p_{0k} \approx q_{0k}$  ( $k = 1, 2$ ), labeled as  $L_{a_0} \parallel L_{b_0}$ . Moreover, the crossover frequency  $f_{sc}$  also logarithmic linearly increases with the flow rate. And the slope of the fitting line is nearly consistent with that of the quadratic denominator coefficient ( $b_2$ ), which is the highest degree of the effective denominator coefficients for the third-order system ( $b_3 = 1$ , Eq. 7).

In summary, the overall third-order system identification for this flow-rate-dependent transport system (microchannel A) could be described by few fitting coefficients. Once determining the flow rate, the transmission characteristics of the biochemical signals transporting in the microchannel are almost known immediately, both in

time-domain and frequency-domain. And once the input is determined, the corresponding approximated output could be received within few seconds.

### 3.4 Fluorescein experimental validation

To verify the log–log linear relationship between the system parameters and the flow rate, and the practicability and accuracy of the approximation by the third-order system experimentally, fluorescein solution with dynamic concentrations mimicking the dynamic biochemical signal was injected into the microfluidic chip. The fluorescent intensities at the inlet of microchannel A and near the cell trap, i.e., the real input and output, were measured simultaneously, after the transmission reached a steady state. The duration of the unstable transmission is related to the flow rate  $Q$  (ESI Fig. S5) and the input frequency  $f_c$  (Fig. 3), wherein the flow rate  $Q$  plays a more critical role. Higher the flow rate, shorter the lasting time for reaching stable transmission. Generally, the lasting time for reaching

a stable state is less than 200 s when  $Q > 2\mu\text{L}/\text{min}$  (see ESI Fig. S6). Herein, all the data were recorded 3min after turning on the syringe pumps. Then, the input was transported into the identified optimal third-order system to compare its output with the real one. The system parameters were calculated by Eqs. 8 and 9. Figure 9 shows the comparisons under various experimental conditions, including two flow rates, three input frequencies, and three waveform types. Overall, the identified outputs almost lie on the experimental ones at all experimental conditions, especially for the higher  $Q$ , lower  $f_c$ , and simpler waveform case. On other conditions, the experimental data contain more high-frequency components which are probably ambient noises; they are filtered when transporting in the third-order system; thus, the identified outputs look more smooth. While, the crucial features, such as the frequency and amplitude, are all captured. Therefore, in terms of both simulation and experiment, this transport system within the single-cell-trapping microchannel A can be simplified as a linear third-order system, and the system parameters are definitely quantified by the flow rate.

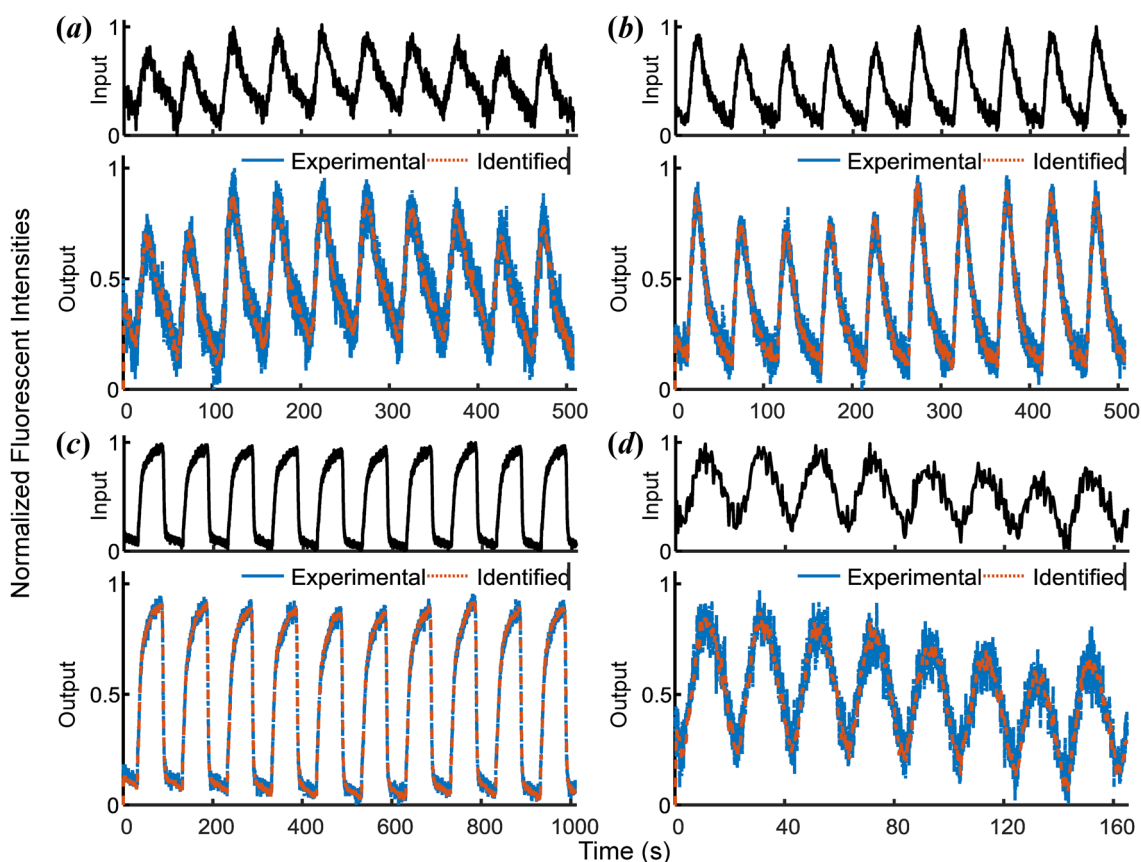


**Fig. 9** Fluorescein validations under various experimental conditions, including three input frequencies, and three waveform types, under two flow rates. **a**  $Q = 6\mu\text{L}/\text{min}$ ,  $f_c = 0.02\text{Hz}$ , pulse-like; **b**

$Q = 12\mu\text{L}/\text{min}$ ,  $f_c = 0.02\text{Hz}$ , pulse-like; **c**  $Q = 12\mu\text{L}/\text{min}$ ,  $f_c = 0.01\text{Hz}$ , square-like; **d**  $Q = 12\mu\text{L}/\text{min}$ ,  $f_c = 0.05\text{Hz}$ , sine-like. Sampling time: 0.07459 s

## 4 Discussion

Analyzing the transmission characteristics of the dynamic biochemical signals transporting in the microchannels simply and rapidly is prerequisite for precisely controlling and quantitatively loading biochemical stimulations to cells in the investigation of single cell dynamics (Na et al. 2020; Recktenwald et al. 2021). However, most mass-transfer microchannels applied to single cell analysis are complicated nonlinear transport systems without definite transfer functions (Yu et al. 2019). Thus, the mass-transfer process with the microchannels could be analyzed only be time-consuming numerical approaches; but the incapacity of precise control still remains due to the unclarity of the system transfer function. In this work, we propose a simplification method to approximate the complicated transport system within a single-cell-trapping microchannel by linear low-order systems. The number of the linear system parameters (zero number and pole number) is decided with comprehensive considerations of the approximating performance and system complexity, quantified by the distributions and values of averaging-MRE and averaging-MSE, and the system order, at various input and flow conditions, respectively (‡ESI Figs. S3, S4 and Fig. 2). By introducing noise to the input–output data sets, the influence of the uncertainties of relevant individual variables and their propagation into the system identification can be effectively reduced (‡ESI Fig. S3). Then, based on the identified model with consideration of noise, the parameters of the most “cost-effective” system (herein, third-order system with 1 zero) are also confirmed. The overall approximations are satisfactory, basically capturing the crucial features, either for the simpler inputs (Figs. 3–6, ‡ESI Figs. S5) or more complicated signals (Fig. 7). Therefore, simplifying the transmission characteristics of the biochemical signal transporting within a mass-transfer microchannel by a third-order system is highly feasible and effective.

For all the transport systems within microchannels, the system characteristics are governed by the combination of convection diffusion equation and Navier–Stokes equation (Li et al. 2013, 2018; Yu et al. 2019; Recktenwald et al. 2021). Thus, they are flow condition dependent. Herein, we illustrate the explicit functions between the simplified system parameters and the flow rate (Eqs. 8 and 9), based on the linear fitting results in the logarithmic coordinate (Fig. 8). Therefore, the transportations under arbitrary flow rate could be identified precisely and rapidly without the time-consuming simulations. These have been validated experimentally (Fig. 9). Besides, the corresponding crossover frequency  $f_{sc}$  could be also confirmed, which is critical to provide meaningful suggestion on the

selection of stimulation frequency experimentally. Based on all these results under steady flow, we could speculate that the transporting process under pulsatile flow within this microchannel would probably be approximated by a third-order system as well, and the system parameters might be time-dependent, that is,  $a_i = F_a[Q(t)] = F_a(t)$  and  $b_j = F_b(t)$ . Especially, for the pulsatile flow with very low frequency or tiny amplitude, or under the assumption of quasi-steady flow, they might be constant, that  $a_i/b_j \approx F_{a/b}(Q_0)$ , where  $Q_0$  is the average flow rate of the pulsatile flow. It is a meaningful topic that we are going to further investigate it deeply.

In addition, as mentioned above, the most “cost-effective” system herein is the third-order system with 1 zero. While it is not the only option. In case of the identifying expectation with high goodness of approximation and extremely tiny error (such as MRE < 1% or lower), a linear system with higher order could be picked specifically. In this work, the approximations of the transport system within the single-cell-trapping microchannel A by second-order to fourth-order systems are all investigated (Fig. 2, ‡ESI Figs. S4, S5). Similar to the third-order system, their system parameters also approximately linearly vary with the flow rate in logarithmic coordinate, as well as the corresponding crossover frequencies of the system (‡ESI Figs. S7). More importantly, the fitting line slopes of the numerator and denominator coefficients with the same order are approximately identical, i.e.,  $L_{a_i} \parallel L_{b_i}$ ; and  $a_0$  and  $b_0$  are geometrically indistinguishable,  $L_{a_0} \parallel L_{b_0}$ . Similarly, the fitting line of the crossover frequency is parallel to that of the highest degree of the effective denominator coefficient,  $L_{f_{sc}} \parallel L_{b_{(n_p-1)}}$ . That is, the numerator coefficients  $a_i$  and denominator coefficients  $b_j$  of the identified system are intrinsically relevant, regardless of the system order. It probably is an inherent characteristic of this transport system (single-cell-trapping microchannel A). More studies focus on system features and the corresponding physical meanings should be further stressed to decipher these phenomena. It would be also beneficial to better understand the transmission characteristics of the dynamic biochemical stimulation within it.

Theoretically, the simplifying approach proposed in this work could be universally applicable to other transport systems, as long as several effective input and output data (simulations or experiments) are pre-known. And more diversified input–output data (multiple frequency components, varying amplitude, etc.) would lead to better approximation performance. Definitely, the system characteristics, such as the relationships between the parameters and flow rate, should be individually distinct. It is another focalization to be explored in the subsequent studies to verify the universality of this simplification method.

## 5 Conclusions

In this work, a simple and effective approach for simplifying the transmission characteristics of the dynamic biochemical signal transporting within a single-cell-trapping microchannel under steady flows by linear low-order systems has been proposed. According to the study objectives, specific linear system with distinct orders could be purposefully decided. The third-order system is labeled as the most “cost-effective” one herein due to the satisfactory approximation effects and system simplicity. Moreover, it is found that the parameters, gain and crossover frequency of this identified third-order system all vary linearly with the flow rate of steady flow in the logarithmic coordinate, which has also been validated experimentally. The simplifying approach could be universally applied to other transport systems theoretically. Therefore, this simple and convenient method can be expected to improve further research on the precise loading and controlling extracellular conditions *in vitro* in single cell analysis.

**Supplementary Information** The online version contains supplementary material available at <https://doi.org/10.1007/s10404-023-02623-w>.

**Acknowledgements** The research reported here was supported by the National Natural Science Foundation of China (Grant Nos. 31971243, 11902066) and the Fundamental Research Foundation for the Central Universities in China (Grant Nos. 2021-YGJC-09, DUT20YG113).

**Author Contributions** MY designed, modeled, and analyzed results, and prepared manuscript; C-DX and S-XL reviewed the manuscript; Y-JL and K-RQ conceived and supervised the research, and also reviewed the manuscript. All authors have read and agreed to the published version of the manuscript.

## Declarations

**Conflict of interest** There are no conflicts to declare.

## References

- Altschuler SJ, Wu LF (2010) Cellular heterogeneity: do differences make a difference? *Cell* 141(4):559–563
- Azizi F, Lu H, Chiel HJ, Mastrangelo CH (2010) Chemical neurostimulation using pulse code modulation (pcm) microfluidic chips. *J Neurosci Methods* 192(2):193–198
- Azizi F, Mastrangelo CH (2008) Generation of dynamic chemical signals with pulse code modulators. *Lab Chip* 8(6):907–912
- Bai E-W (2008) Non-parametric nonlinear system identification: a data-driven orthogonal basis function approach. *IEEE Trans Autom Control* 53(11):2615–2626
- Bai Y, Patil SN, Bowden SD, Poulter S, Pan J, Salmond GP, Welch M, Huck WT, Abell C (2013) Intra-species bacterial quorum sensing studied at single cell level in a double droplet trapping system. *Int J Mol Sci* 14(5):10570–10581
- Beard DA (2001) Taylor dispersion of a solute in a microfluidic channel. *J Appl Phys* 89(8):4667–4669
- Beard DA (2001) Response to “comment on ‘taylor dispersion of a solute in a microfluidic channel’”. *J Appl Phys* 90(12), 6555–6556 (2001)
- Brownlee M, Hirsch IB (2006) Glycemic variability: A hemoglobin a1c - independent risk factor for diabetic complications. *JAMA* 295(14):1707–1708
- Chen P, Guo Y, Feng X, Yan S, Wang J, Li Y, Du W, Liu B-F (2017) Microfluidic chemical function generator for probing dynamic cell signaling. *Anal Chem* 89(17):9209–9217
- Chen P, Yan S, Wang J, Guo Y, Dong Y, Feng X, Zeng X, Li Y, Du W, Liu B-F (2018) Dynamic microfluidic cytometry for single-cell cellomics: high-throughput probing single-cell-resolution signaling. *Anal Chem* 91(2):1619–1626
- Chen Z-Z, Yuan W-M, Aziz A, Gao Z-M, Zeng D-P, Liu B, Qin K (2017) Transfer characteristics of dynamic biochemical signals in non-reversing pulsatile flows in a shallow y-shaped microfluidic channel: signal filtering and nonlinear amplitude-frequency modulation. *Appl Math Mech* 38(10):1481–1496
- Chingozha L, Zhan M, Zhu C, Lu H (2014) A generalizable, tunable microfluidic platform for delivering fast temporally varying chemical signals to probe single-cell response dynamics. *Anal Chem* 86(20):10138–10147
- Gao D, Jin F, Zhou M, Jiang Y (2019) Recent advances in single cell manipulation and biochemical analysis on microfluidics. *Analyst* 144(3):766–781
- Garcia S, Sunyer R, Olivares A, Noailly J, Atencia J, Trepast X (2015) Generation of stable orthogonal gradients of chemical concentration and substrate stiffness in a microfluidic device. *Lab Chip* 15(12):2606–2614
- Guo Y, Gao Z, Liu Y, Li S, Zhu J, Chen P, Liu B-F (2020) Multichannel synchronous hydrodynamic gating coupling with concentration gradient generator for high-throughput probing dynamic signaling of single cells. *Analytical Chemistry* 92(17):12062–12070
- Guo F, Mao Z, Chen Y, Xie Z, Lata JP, Li P, Ren L, Liu J, Yang J, Dao M et al (2016) Three-dimensional manipulation of single cells using surface acoustic waves. *Proc Natl Acad Sci* 113(6):1522–1527
- Heath JR, Ribas A, Mischel PS (2016) Single-cell analysis tools for drug discovery and development. *Nat Rev Drug Discov* 15(3):204–216
- Kim Y, Song J, Lee Y, Cho S, Kim S, Lee S-R, Park S, Shin Y, Jeon NL (2021) High-throughput injection molded microfluidic device for single-cell analysis of spatiotemporal dynamics. *Lab Chip* 21(16):3150–3158
- Kniss-James AS, Rivet CA, Chingozha L, Lu H, Kemp ML (2017) Single-cell resolution of intracellular t cell  $Ca^{2+}$  dynamics in response to frequency-based  $H_2O_2$  stimulation. *Integr Biol* 9(3):238–247
- Lam Y, Chen X, Yang C (2005) Depthwise averaging approach to cross-stream mixing in a pressure-driven microchannel flow. *Microfluid Nanofluid* 1(3):218–226
- Lee D-H, Li X, Ma N, Digman MA, Lee AP (2018) Rapid and label-free identification of single leukemia cells from blood in a high-density microfluidic trapping array by fluorescence lifetime imaging microscopy. *Lab Chip* 18(9):1349–1358
- Li Y-J, Cao T, Qin K-R (2018) Transmission of dynamic biochemical signals in the shallow microfluidic channel: nonlinear modulation of the pulsatile flow. *Microfluid Nanofluid* 22(8):1–13
- Li Y-J, Li Y-Z, Cao T, Qin K-R (2013) Transport of dynamic biochemical signals in steady flow in a shallow y-shaped microfluidic channel: effect of transverse diffusion and longitudinal dispersion. *J Biomech Eng* 135(12):121011
- Lipp C, Uning K, Cottet J, Migliozi D, Bertsch A, Renaud P (2021) Planar hydrodynamic traps and buried channels for bead and cell trapping and releasing. *Lab Chip* 21(19):3686–3694
- Na J-T, Xue C-D, Li Y-J, Wang Y, Liu B, Qin K-R (2020) Precise generation of dynamic biochemical signals by controlling the

- programmable pump in a y-shaped microfluidic chip with a “christmas tree” inlet. *Electrophoresis* 41(10–11):883–890
- Recktenwald SM, Wagner C, John T (2021) Optimizing pressure-driven pulsatile flows in microfluidic devices. *Lab Chip* 21:2605–2613
- Roper MG (2016) Cellular analysis using microfluidics. *Anal Chem* 88(1):381–394
- Silverio V, López-Martínez MJ, Franco F, Amaral M, Gaspar J, Cardoso S, Freitas PP (2017) On-chip magnetic nanoparticle manipulation and trapping for biomedical applications. *IEEE Trans Magn* 53(11):1–6
- Song J, Ryu H, Chung M, Kim Y, Blum Y, Lee SS, Pertz O, Jeon NL (2018) Microfluidic platform for single cell analysis under dynamic spatial and temporal stimulation. *Biosens Bioelectron* 104:58–64
- Spiller DG, Wood CD, Rand DA, White MR (2010) Measurement of single-cell dynamics. *Nature* 465(7299):736–745
- Tan H, Hu H, Huang L, Qian K (2020) Plasmonic tweezers for optical manipulation and biomedical applications. *Analyst* 145(17):5699–5712
- Tay S, Hughey JJ, Lee TK, Lipniacki T, Quake SR, Covert MW (2010) Single-cell *nf- $\kappa$ b* dynamics reveal digital activation and analogue information processing. *Nature* 466(7303):267–271
- Venkat AN, Vijaysai P, Gudi RD (2003) Identification of complex non-linear processes based on fuzzy decomposition of the steady state space. *J Process Control* 13(6):473–488
- Wen L, Tang F (2018) Boosting the power of single-cell analysis. *Nat Biotechnol* 36(5):408–409
- Xie Y, Wang Y, Chen L, Mastrangelo C (2008) Fourier microfluidics. *Lab Chip* 8(5):779–785
- Yu M, Chen Z-Z, Xiang C, Liu B, Xie H, Qin K-R (2016) Microfluidic-based single cell trapping using a combination of stagnation point flow and physical barrier. *Acta Mech Sin* 32(3):422–429
- Yu M, Li Y-J, Shao J-Y, Qin K-R (2019) Transport of dynamic biochemical signals in a microfluidic single cell trapping channel with varying cross-sections. *Eur Phys J E* 42(3):1–12

**Publisher's Note** Springer Nature remains neutral with regard to jurisdictional claims in published maps and institutional affiliations.

Springer Nature or its licensor (e.g. a society or other partner) holds exclusive rights to this article under a publishing agreement with the author(s) or other rightsholder(s); author self-archiving of the accepted manuscript version of this article is solely governed by the terms of such publishing agreement and applicable law.